Journal of Power Sources 271 (2014) 291–297

Contents lists available at ScienceDirect

Journal of Power Sources

journal homepage: www.elsevier.com/locate/jpowsour

Novel dual-salts electrolyte solution for dendrite-free lithium-metal based rechargeable batteries with high cycle reversibility

Rongrong Miao, Jun Yang*, Xuejiao Feng, Hao Jia, Jiulin Wang, Yanna Nuli

School of Chemistry and Chemical Engineering, Shanghai Jiao Tong University, 800 Dongchuan Road, Shanghai 200240, China

HIGHLIGHTS

- A new dual-salts electrolyte solution has been explored for lithium metal anode.
- Excellent cycling performance and dendrite-free lithium deposit have been achieved.
- Low voltage polarization and favorable lithium morphology can be retained even at high current density of 10 mA cm^{-2}.

GRAPHICAL ABSTRACT

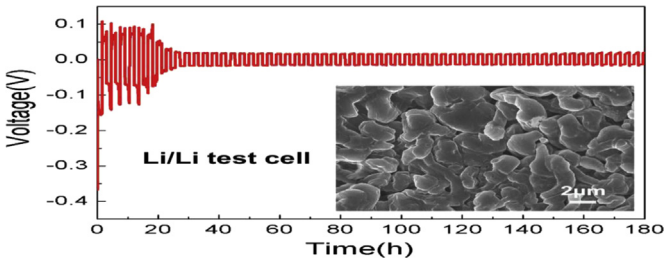

ARTICLE INFO

Article history:
Received 22 March 2014
Received in revised form
24 July 2014
Accepted 2 August 2014
Available online 10 August 2014

Keywords:
Dual-salts electrolyte
Lithium dendrite
Cycle efficiency
High current density
Lithium-metal rechargeable battery

ABSTRACT

Metallic lithium is the most promising negative electrode for high energy rechargeable batteries due to its extremely high specific capacity and the lowest redox potential. However, the low cycle efficiency and lithium dendrite formation during charge/discharge processes consistently hinder its practical application. Here a new dual-salts electrolyte composed of $Li[N(SO_2F)_2]$ and $Li[N(SO_2CF_3)_2]$ has been explored to simultaneously cope with these two problems. Under the unique protection of solid electrolyte interphase (SEI) film formed in this electrolyte solution and the improvement in Li crystal growth pattern, high cycle efficiency of *ca.* 99% and dendrite-free Li deposit have been achieved. Moreover, the excellent cycling performance and favorable lithium morphology can be retained even at high current density of 10 mA cm^{-2}. This study will greatly promote the development of Li-metal rechargeable batteries with high power and high energy density.

1. Introduction

Although lithium-ion batteries are being widely used as power sources for portable devices and (hybrid) electric vehicles, the limited energy density of less than 200 Wh kg^{-1} by using conventional graphite anode material is still unable to meet the exigent demand for smaller and lighter devices and more powerful electric vehicles [1]. Driving by this challenge, more and more researchers pay attention to Li-metal-based rechargeable battery systems [2]. For instance, lithium–sulfur battery has been intensively investigated due to its high theoretical energy density of 2600 Wh kg^{-1} [3,4]. Moreover, a higher theoretical value is obtainable for lithium–air battery [5]. Both the systems use lithium metal as anode, which provides extremely high theoretical specific capacity (3800 mAh g^{-1}) and the lowest redox potential (−3 V *vs.* standard hydrogen electrode, SHE) [6]. Based on its unique advantage, metallic Li is becoming the most promising anode candidate for next generation energy storage systems. However, highly thermodynamic instability of lithium to organic solvents causes low cycle efficiency and lithium dendrite formation during discharge/charge processes, which are two major obstacles for its practical application [7,8]. The growth of lithium dendrites in continuous cycling

* Corresponding author. Tel./fax: +86 21 5474 7667.
E-mail address: yangj723@sjtu.edu.cn (J. Yang).

http://dx.doi.org/10.1016/j.jpowsour.2014.08.011
0378-7753/

may lead to internal short circuit and further incur fire or other safety problems, while the low cycling efficiency will result in short cycle life and final battery failure [9,10].

Beginning in the early 1970s, various attempts from the Li surface protection to electrolyte selection have been made to solve these two key problems [11,12]. Although a great progress has been made to address these issues, few approaches are successful to solve all these problems at the same time. For example, some additives (*e.g.* CO_2 [13], SO_2 [14,15], 2-Meyhyfuran [16], *etc.*) in liquid electrolytes are helpful to gain relatively long cycle life, but lithium dendrite formation nature does not be changed. Compared with the liquid electrolyte, PEO-based one is advantageous for its elastic property and good compatibility with lithium, but the dendrite growth still could not be suppressed fundamentally and only the onset time of lithium dendrite formation can be prolonged to some extent [17–19]. In addition, its blocking to lithium dendrite growth seems to be invalid at elevated temperature due to losing mechanical strength of PEO [7,20]. A significant breakthrough has been achieved by Aurbach group [21]. The liquid electrolyte system containing 1,3-dioxolane (DOL), $LiAsF_6$ and tributylamine in trace amount as a stabilizer shows dendrite-free lithium morphology and almost 100% Li deposition–dissolution efficiency. Unfortunately, it still faces some application obstacles. At charging rate higher than 1.5 mA cm^{-2}, the cycle life is limited [22,23]. Moreover, the $LiAsF_6$ salt is toxic. Similarly, the newly proposed electrolyte with $CsPF_6$ as additive can effectively suppress lithium dendrite with a columbic efficiency of more than 98% [24]. However, the additive can only be effective to prevent the dendrite growth at limited current densities. Too large a current density will induce a large voltage drop which may compel the additives to be co-deposited with Li and thereby diminish the effect of the additives [7]. In short, the up-to-date results are still unsatisfactory for practical application. It is necessary to design new electrolyte systems to cope with both the low coulombic efficiency and dendrite formation at adequate current rate.

As is generally known, SEI layer on lithium metal strongly affects Li deposit morphology and cycling performance [25]. As the main source of organic composition in SEI film, the choice of solvents in electrolytes is very important for lithium anode. The commonly used liquid electrolyte solutions adopt three families of solvents, namely, ethers, esters, and alkyl carbonates. It is already known from previous studies that lithium is not passivated in ester or alkyl carbonate (*e.g.* BL, PC, DMC, *etc*) based electrolytes for lack of stable or flexible solid surface films on lithium [26–28]. With regard to the compatibility to highly reactive Li metal, ethers seem to be a good choice for its relatively low oxidation state [29,30]. Particularly, the cyclic ether solvents are superior to stabilize the surface of Li metal by forming an elastic surface layer through the ring-opening reaction [31]. For example, the electrolyte with 1,3-dioxolane (DOL) as solvent and $LiAsF_6$ as lithium salt shows the distinct superiority in cycling stability because of the formation of flexible and insoluble polydioxolane oligomers on the lithium surface, which could accommodate the morphological change of the Li-metal during cycling [21,22]. Based on the above results, we choose DOL as main solvent. On the other hand, lithium salts also play a critical role for forming a thin, compact and uniform SEI film. However, compared to the variety of solvents, the Li salts suitable for lithium metal-based systems are very limited [13]. Li $[N(SO_2CF_3)_2]$ (LiTFSI) is often used in Li–S batteries and also ionic liquids containing $TFSI^-$ anion have proven helpful for improving lithium metal cycling efficiency, but the tolerance of large current density of Li anode is still limited [13,32,33]. In view of that another sulfonyl imide salt Li$[N(SO_2F)_2]$ (LiFSI) possesses high ionic conductivity and good compatibility with lithium [34–36], we conceive the combination of LiFSI and DOL for a new electrolyte to match Li metal anode. However, it has been found in our experiment that the solubility of LiFSI is very low in DOL solvent and open-ring polymerization of DOL is easily induced. Although adding dimethoxymethane (DME) as co-solvent can improve the solubility of LiFSI greatly, its stability in DOL–DME co-solvent is still poor.

In the present work, combined with the high stability of LiTFSI in DOL solvent system, a novel dual-salts electrolyte solution mating organic LiTFSI to inorganic LiFSI is designed and prepared, in which LiFSI not only provides high conductivity, but also dominates the interfacial behavior, while LiTFSI acts as stabilizer and conducting agent. Both the anion structures are given in the followed (I) and (II). This simple but effective dual-salts electrolyte system shows steady and high coulombic efficiency and dendrite-free lithium deposition even at high current density. The possible function mechanism is explored and discussed.

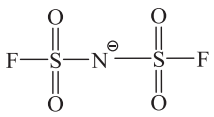

(Ⅰ) FSI^- anion

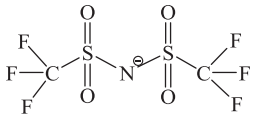

(Ⅱ) $TFSI^-$ anion

2. Experimental

2.1. Preparation of dual-salts electrolyte solution

All the raw materials used in experiments are Li battery grade. LiTFSI and LiFSI were obtained from Capchem. Co. Ltd. and Suzhou Fluolyte. Co. Ltd, respectively. Anhydrous 1,3-dioxolane (DOL) and dimethoxymethane (DME) were obtained from Aldrich, Inc. The experimental work was carried out in an Ar-filled dry glove box (MB-10 compact, MBRAUN) containing less than 1 ppm water and O_2. Firstly, Anhydrous DOL was mixed with anhydrous DME in 2:1 volume ratio, then 0.5 M LiTFSI was dissolved in the mixed solvent. Finally, 0.5 M LiFSI was slowly added to the above solution and further stirred for 12 h at room temperature in the glove box to form the electrolyte solution. The mole ratio of Li^+ from these two kinds of salts was 1:1. The total concentration of dual-salts was 1 mol L^{-1} and the water content in the final electrolyte is 30.8 ppm measured by coulometric KF titrator (C30, Mettler Toledo).

2.2. Electrode characterization

The morphologies of lithium metal electrodes were observed by FEI Nova Nano-scanning electron microscope (SEM). Firstly, cells were disassembled in the glove box and then the obtained electrodes were thoroughly washed by anhydrous DME to remove any electrolyte salt residuals. To avoid exposure to air, the dried samples were sealed in an air-isolating container and transferred quickly into the SEM equipment under the protection of Ar flow.

The X-ray photoelectron spectroscopy (XPS) analysis was performed using a Kratos Axis UltraDLD spectrometer (Kratos Analytical-A Shimadzu Group Company) with monochromatic Al Kα source (1486.6 eV). Before transferring the samples to the equipment, an air-isolating container with protective Ar flow was used to avoid moisture/air exposure. Under slot mode, the analysis area was 700 × 300 μm and analysis chamber pressure was less than 5×10^{-9} Torr. The binding energy was calibrated according to the C 1s peak (284.8 eV) of adventitious carbon on the analyzed sample surface.

2.3. Electrochemical measurements

The $LiFePO_4$ electrode and sulfur composite electrode with S content of 38.7% were fabricated by mixing active material, Super P conductive carbon black (40 nm, Timical) and binder in weight ratio of 80:10:10 for electrolyte compatibility measurement. The binders used in $LiFePO_4$ electrode and sulfur composite electrode were poly(vinylidene difluoride) and cyclodextrin respectively. The sulfur composite was synthesized by pyrolysis of a mixture of PAN and sulfur according to our previous report [37]. After casting the slurry on Al (for $LiFePO_4$) and foam Ni (for S-based) current collectors, the electrodes were dried at 65 °C in vacuum for 4 h. The coin cells CR2016 were assembled with the above electrodes, pure lithium foil as counter electrode and ENTEK ET 20–26 (PE, thickness: 20 μm) as separator in an Ar-filled dry glove box containing less than 1 ppm water and O_2. The discharge and charge measurements at room temperature were carried out on a LAND-CT 2001A Battery Test System (Wuhan, China).

The coulombic efficiency and deposition–dissolution performance of lithium were examined using Li/electrolyte/stainless steel (SS) cells with the separator ENTEK ET 20–26 and different electrolyte solutions. During this experiment, a constant deposition current density of 0.25 mA cm^{-2} was passed through the cell for 2.5 h, and then the same dissolution current density was applied until the cut-off voltage of 1.2 V *vs.* Li. The process of Li deposition–dissolution at high current density of 10.0 mA cm^{-2} was conducted by using symmetrical Li/Li cell, which was cycled with charge amount of 54 C cm^{-2} for each cycle.

Cyclic voltammogram was measured with a three-electrode cell system using a CHI604A electrochemical workstation (Shanghai, China). The working electrode was Pt disc electrode (area: 0.0314 cm^2) and lithium slice served as counter electrode and reference electrode (RE). The Pt disc electrode was polished with Al_2O_3 powder and rinsed with alcohol before use.

The ionic conductivity of the electrolyte solution was measured using a FE30 conductivity meter and an InLab 710 conductivity measuring cell (Mettler Toledo, Switzerland) by inserting the InLab 710 conductivity electrode in solution after calibration.

The A.C. impedance spectroscopy of Li–Li symmetric cells with different electrolyte solutions and the above-mentioned separator were measured using a frequency response analyzer (CHI660C) with an electrochemical interface in the frequency range from 1 MHz to 0.01 Hz.

3. Results and discussion

3.1. Coulombic efficiency and galvanostatic cycling performance

In order to examine the coulombic efficiency of lithium deposition/dissolution processes, galvanostatic cycling experiments were conducted. The efficiency was calculated according to the ratio of the charge amount of Li dissolution to that of Li deposition on stainless steel (SS). It can be observed from Fig. 1a that the first columbic efficiency reaches to 91.6% in dual-salts solution and after several cycles it becomes stable, approximating 99%, which is much higher than those in conventional electrolytes for Li-ion batteries and single salt LiTFSI electrolyte system. For carbonate electrolyte with 1 M $LiPF_6$, the over-voltage for Li deposition and dissolution is high up to ~44 mV and the deposition voltage shows an ascending tendency with time (Fig. 1b). After 75 cycles the deposition voltage drastically fluctuates with high polarization. The same tendency can also be found in electrolyte with single lithium salt LiTFSI (Fig. 1c). The electrolyte with dual-salts shows excellent lithium deposition/dissolution performance (Fig. 1d). The over-voltages for

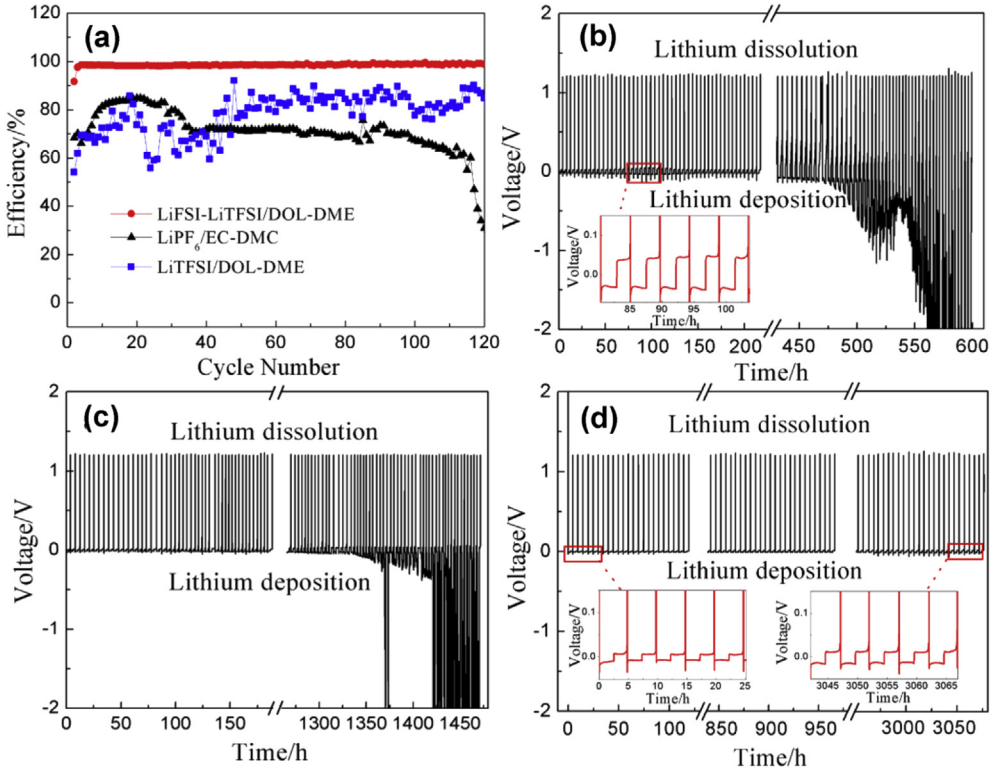

Fig. 1. Lithium deposition–dissolution performances in Li/electrolyte/SS cells. (a) Coulombic efficiency *vs.* cycle number for different electrolyte solutions. (b, c, d) Galvanostatic voltage–time curves respectively in $LiPF_6$/EC–DMC, LiTFSI/DOL–DME and LiFSI–LiTFSI/DOL–DME solutions. Each dissolution and deposition of lithium-metal was performed at 25 °C under constant deposition current of 0.25 mA cm^{-2} for 2.5 h (*ca.* 4.5C), and then the same dissolution current density was applied until the cut-off voltage of 1.2 V *vs.* Li.

lithium deposition/dissolution are small (<6.8 mV) and stable. Even after 3000 h' cycling the over-voltage is still stable and below 15 mV (see the inset in Fig. 1d). The difference in the over-voltage is associated with the interfacial resistance and electrode reaction involving charge transfer, which are strongly influenced by compositions of the surface film and electrolyte. The interfacial resistance obtained by the A.C. impedance measurement is 88.6 Ω cm^2 for Li/Li symmetric cells containing the LiFSI–LiTFSI electrolyte after stabilization for 4 h, compared with 195.0 Ω cm^2 in $LiPF_6$ electrolyte. The high cycle stability and electrochemical reversibility of lithium deposition/dissolution demonstrates a new avenue for lithium metal anode used in nonaqueous liquid electrolyte.

3.2. Observation of Li morphologies deposited in different electrolytes

Another advantage of this dual-salts electrolyte is the effective suppression of lithium dendrite. The surface morphologies of Li electrodes cycled in different solutions are shown in Fig. 2. In view of the fact that Li deposition at current density above 1 mA cm^{-2} is highly dendritic in most of the commonly used nonaqueous electrolyte solutions [22], relatively high current density of 2 mA cm^{-2} was used in this experiment to observe the surface morphology of Li deposit. After 10 cycles, the pronounced differences can be observed from Fig. 2. In conventional carbonate based electrolyte, the lithium deposit is either dendritic or spongy (Fig. 2a and b). Whereas, lithium deposit from the dual-salts electrolyte shows smooth solid particle morphology (Fig. 2c and d). To further gain an insight into the structure of Li deposit, its cross-section morphology was observed. As shown in Fig. 2e, the mossy and needle-like lithium with the incompact configuration can be easily identified after 5 cycles in the conventional electrolyte. In particular, a long dendrite near 10 μm directly grown from Cu substrate is observable. On the contrary, Li deposit obtained from the dual-salts electrolyte exhibits a neat and compact particle array (Fig. 2f), which offers a basic condition for forming a high quality SEI layer. The apparent morphology transformation could be attributed to the unique surface chemistry and interfacial property, which is adjustable via the electrolyte composition. As concerning only electrolyte solvents, due to the existence of oligomers of polydioxolane (partial polymerization and reduction of solvent DOL), functioning as an

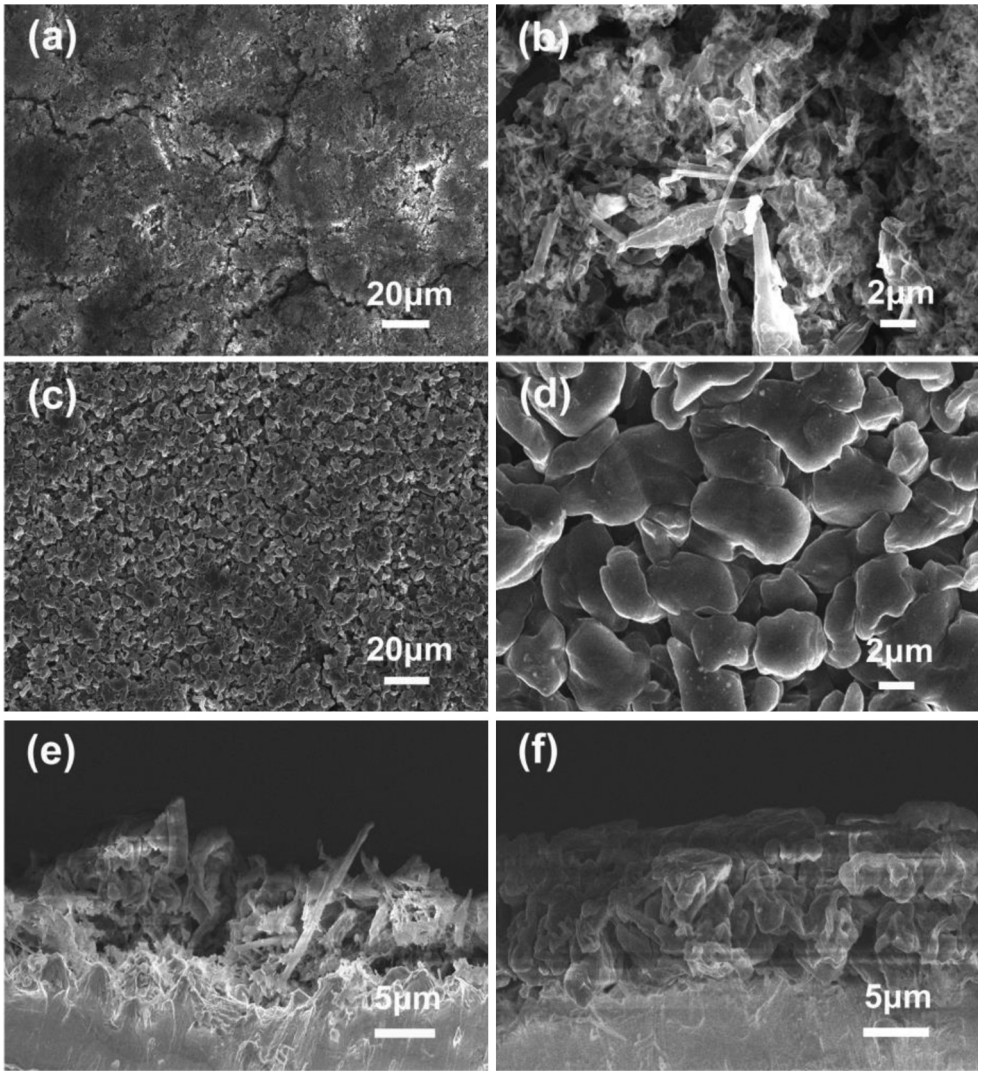

Fig. 2. SEM micrographs of Li electrodes after 10 cycles in Li/electrolyte/Li symmetric cells with 4C per process at 2 mA cm^{-2}. (a, b) in a conventional $LiPF_6$/EC-DMC electrolyte. (c, d) in LiFSI–LiTFSI/DOL–DME electrolyte. The final state is lithium deposition. (e, f) Cross-section micrographs of metallic lithium electrodeposited on Cu substrate after 5 cycles in conventional $LiPF_6$/EC-DMC electrolyte and in LiFSI–LiTFSI/DOL–DME electrolyte. The first deposition: 3 C cm^{-2}, during followed cycles: 1 C cm^{-2} per process at 0.5 mA cm^{-2}, the final state is lithium deposition on Cu substrate.

elastomer [21], a flexible surface film can be formed in the dual-salts electrolyte system, which could better accommodate the volume changes upon repeated Li deposition–dissolution processes and benefit the uniform and compact lithium deposits. Whereas, the surface film formed from $LiPF_6$ solution is mainly based on Li alkyl carbonate film ($ROCO_2Li$, ROLi, $RCOO_2Li$, etc.), combing with some salt reduction products [26], which cannot accommodate the morphological change of the Li surface during cycling, and thus may be easy to break down, leading to non-uniform current density distribution and lithium dendrite formation. This incompact and dendric Li deposit may further degrade the quality of SEI film and induce more side reaction between fresh deposited lithium and electrolyte, which results in the low and unstable cycling efficiency. In addition, the reiterative repair of the SEI film makes it thicker, leading to the larger interfacial resistance and higher over-potential as shown in Fig. 1.

3.3. Lithium cycle performance at high current density

In general, low current density will not bring on notable Li dendrite formation. High-rate performance is still a big challenge before practical application of Li metal anode in liquid electrolyte due to the dendrite growth. To evaluate the feasibility of this dual-salts electrolyte towards practical power source application, the tolerance of large current density is indispensable. Fig. 3 shows lithium cycling performance with high current density of 10 mA cm^{-2} and sufficient charge amount of 54 C cm^{-2} (*i.e.* 15 mAh cm^{-2}), which is much higher than that of conventional Li-ion cell (3.7 mAh cm^{-2}). Obviously, in this binary salts electrolyte system, the over-voltage tends to be low (*ca.* 20 mV) and extremely stable after the initial several cycles of relatively higher polarization, which may be associated with the interfacial activation and SEI formation (Fig. 3a). In contrast, the over-voltage is unstable and over 400 mV in the LiTFSI electrolyte (Fig. 3b). The fast electrode kinetics in this new electrolyte is supported by its high ionic conductivity (10.22 mS cm^{-1}) and the favorable interfacial property (the interfacial resistance of 88.6 Ω cm^2 in LiFSI–LiTFSI electrolyte, against 152.7 Ω cm^2 in LiTFSI electrolyte). Moreover, as exhibited in Fig. 3c, lithium dendrite can be avoided after 51 cycles at high current density of 10 mA cm^{-2} and large charge amount of 54 C cm^{-2}. The outstanding rate performance of lithium electrode is very significant for the development of high power rechargeable batteries.

3.4. Discussion for the possible function mechanism

In view of small difference of ionic conductivity between the present LiFSI–LiTFSI electrolyte and the conventional $LiPF_6$ electrolyte, the dendrite-free lithium deposition at high current density can not be explained by the fast ionic conduction. In order to better understand the effect of co-salt LiFSI on the Li deposit structure, typical high-resolution region XPS spectra were taken to compare the composition of lithium surface cycled in LiTFSI electrolyte and in LiFSI–LiTFSI electrolyte. The XPS results shown in Fig. 4a indicate a clear difference arising from the LiFSI effect. The surface composition in LiTFSI electrolyte is more complicated. According to the reaction scheme proposed by Aurbach [13], the inorganic composition in surface layer is mainly composed of $Li_2NSO_2CF_3$, $Li_yC_2F_x$, LiF, $Li_2S_2O_4$, Li_2S, *etc.* The fluorine-containing species are dominated by a series of $TFSI^-$ reduction products and small proportion of LiF [38], which is validated by our experiment result (Fig. 4b). In this case, the various $TFSI^-$ anion reduction products precipitated on lithium surfaces form a heterogeneous surface film, which may induce non-uniform current density distribution and eventually uneven lithium deposit. Similarly, the complicated components (*e.g.* LiF, Li_yPF_y, LiOH, Li_2CO_3, etc [26]), along with an organic layer lacking the flexibility, in the surface film formed in ester electrolytes with $LiPF_6$ are also apparently not suitable for lithium metal electrode. Conversely, as shown in Fig. 4a, a much simpler composition of lithium surface is obtained after adding co-salt LiFSI. FSI^- anion may competitively react with lithium due to different bond energy of S–F and S–CF_3.

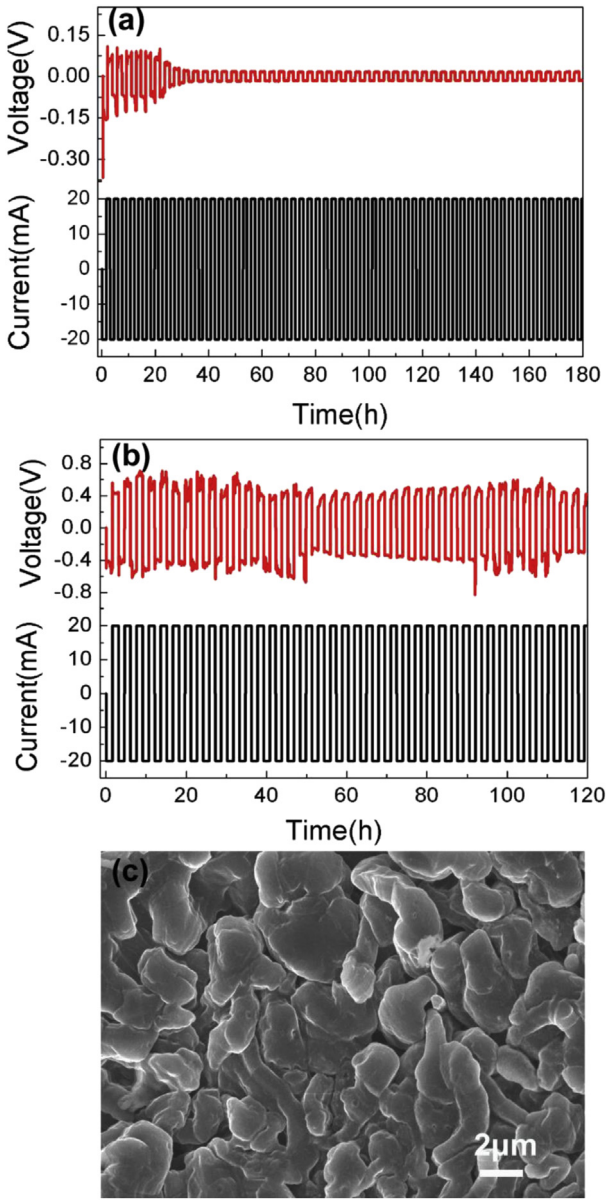

Fig. 3. Cycle performance of lithium electrode at high current density. (a, b) Galvanostatic voltage–time curves for Li/electrolyte/Li symmetric cells respectively in LiFSI–LiTFSI/DOL–DME solution and LiTFSI/DOL–DME solution with current density of 10 mA cm^{-2} and 54 C cm^{-2} per process. (c) SEM micrograph of lithium deposit after 51 cycles in LiFSI–LiTFSI/DOL–DME solution with current density of 10 mA cm^{-2} and 54 C cm^{-2} per process.

Based on the study of Budi et al. [39], the reaction pathway of the FSI^- anion break down is illustrated in Fig. 5. During this competitive reaction of lithium with FSI^- and $TFSI^-$ anion, $-SO_2F$ group in FSI^- is far more reactive than $-SO_2CF_3$ group in $TFSI^-$ toward lithium and the reaction selection largely limits to fluorinated anions firstly. The splitting F ion from the cleavage of S–F bond forms stable LiF, and then the S–N bond in the resulting fragment $F(SO_2)_2N$ is broken under the strong attraction of oxygen

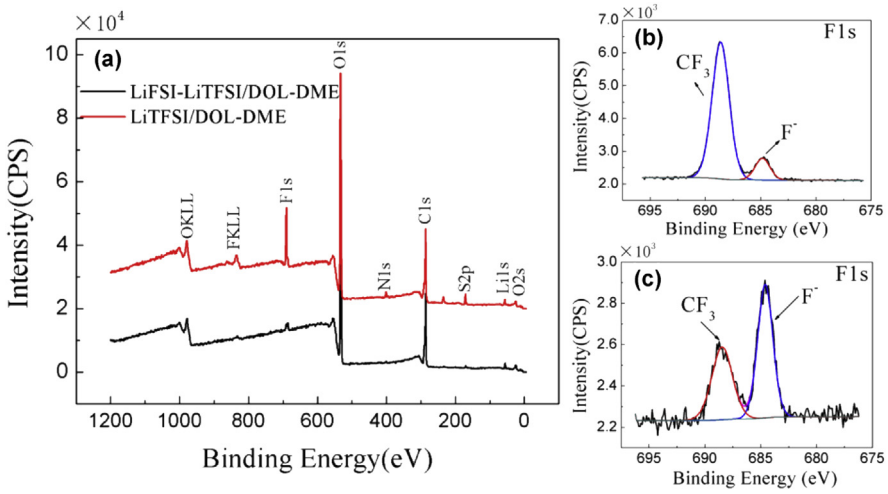

Fig. 4. X-ray photoelectron spectroscopy (XPS) analysis of metallic lithium anodes. (a) The high energy resolution XPS spectra of Li foil surface from Li–Li symmetric cell after 10 cycles in different electrolyte solutions. (b, c) XPS spectra of the F 1s regions of Li surface respectively in LiTFSI/DOL–DME electrolyte and LiFSI–LiTFSI/DOL–DME electrolyte.

atoms to the lithium surface, leading to the formation of SO_2, which promptly runs away from the surface due to the blocking of the LiF-dominating layer earlier formed [39]. That may be the main reason for little formation of sulfur-containing species. Consequently, a simple inorganic composition in the surface film dominated by LiF is formed in the presence of LiFSI (Fig. 4c). Moreover, it is noted that the fluorine content on the surface of Li electrode cycled in the dual-salts electrolyte is only 1.51%, which is much lower than 7.51% on the surface of Li electrodes cycled in LiTFSI electrolyte. Thus, we conclude that a much thinner and dense inorganic layer containing LiF can be formed from this dual-salts electrolyte. This unique surface protection layer suppresses the Li dendrite formation and promotes new deposit morphology towards compact deposition of uniform lithium grains. As reported previously, LiF in surface film was beneficial to the formation of hemispheric lithium particle [40,41].

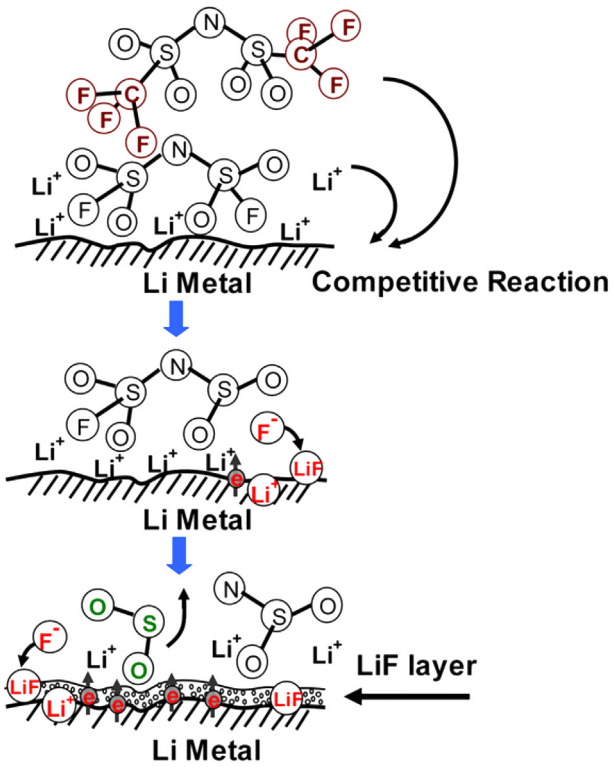

Fig. 5. Schematic illustration of interfacial competitive reaction of FSI anion with lithium metal.

Although LiFSI leads to the favorable deposit morphology, the outstanding electrochemical performance of lithium electrode is not fully dominated by LiFSI. In fact, the cycle efficiency is not high without DOL solvent. It is the synergistic effect of LiFSI and DOL, probably related to the homogeneous inorganic SEI inner-layer and an elastic organic outer-layer (*e.g.* poly-DOL oligomers, CH_3CH_2O-CH_2OLi, HCO_2Li, *etc* [22].) according to the proposed SEI model [42], that successfully suppresses the dendrite formation and enhances the columbic efficiency. Because of the high initial cycle efficiency (91.6%), the SEI film formed from LiFSI–LiTFSI/DOL–DME electrolyte is too thin to be clearly observable by SEM, at least for not long-cycled Li electrode.

3.5. Electrochemical window and compatibility with different cathodes

Besides the cycle reversibility of lithium anode, the electrochemical window and electrolyte–cathode compatibility are also important characters for electrolyte systems. Fig. 6a shows the typical cyclic voltammetry curve of Pt working electrode in the LiFSI–LiTFSI electrolyte. Its electrochemical window towards anodic decomposition is about 3.8 V (*vs.* Li RE). According to a series of contrast experiments (*e.g.* using ester solvents EC and DMC to replace ethers, or changing other lithium-salts such as $LiClO_4$), we find that this low decomposition voltage is mainly due to the ethers solvents. To prove the compatibility of the electrolyte with cathodes under this electrochemical window, Li/$LiFePO_4$ cell and Li/sulfur composite cell were investigated. The 2016-type coin cells comprising the dual-salts electrolyte, Li-mental disc anode and the above cathodes were charged and discharged at room temperature. Fig. 6b and c shows the charge–discharge profiles in the first 3 cycles at 0.1C rate. Almost overlapped curve trends for both the cells confirm excellent electrochemical reversibility with the dual-salts electrolyte.

4. Conclusions

In summary, a new LiFSI–LiTFSI/DOL–DME electrolyte system has been developed to simultaneously address the low coulombic

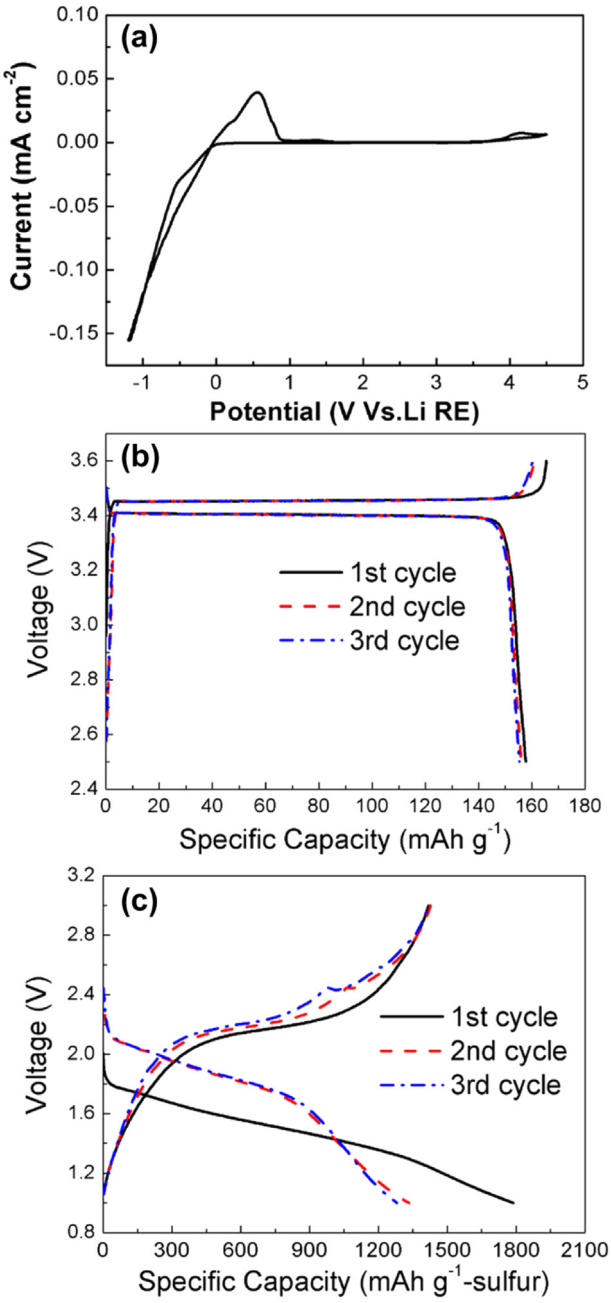

Fig. 6. Electrochemical window and compatibility with different cathodes. (a) Steady-state cyclic voltammogram of the Pt electrode in the dual-salts electrolyte at a scanning rate of 20 mV s^{-1}. (b, c) Galvanostatic charge–discharge profiles of $LiFePO_4$ electrode and sulfur composite (38.7% S) electrode in the dual-salts electrolyte at 0.1C.

efficiency and dendrite formation during charge/discharge processes when using lithium metal as anode. Under the synergistic effect of LiFSI and DOL, probably related to the effective protection of a unique SEI layer, a remarkably enhanced coulombic efficiency (*ca.* 99%) and superior cycle stability of lithium deposition/dissolution are achieved. Furthermore, lithium dendrite is successfully suppressed in this electrolyte by changing the deposit configuration towards neatly and compactly arranged particles. In particular, this favorable Li-deposit morphology and low potential polarization can be maintained even at high current density. On the cathode side, the reversible electrochemical reactions of Li/$LiFePO_4$ cell and Li/sulfur composite cell confirm a good compatibility of the electrolyte with different cathode materials. All the above results prove that this novel electrolyte system has great potential in Li-metal based rechargeable batteries for high energy density.

Acknowledgment

This work was supported by the National Natural Science Foundation of China (No. 21273146) and National Key Basic Research Program of China (No. 2014CB932303).

References

[1] M. Armand, J.-M. Tarascon, Nature 451 (2008) 652–657.
[2] K. Xu, Chem. Rev. 104 (2004) 4303–4418.
[3] J. Wang, J. Yang, J. Xie, N. Xu, Adv. Mater. 14 (2002) 963–965.
[4] X. Ji, S. Evers, R. Black, L.F. Nazar, Nat. Commun. 2 (2011) 325.
[5] P.G. Bruce, S.A. Freunberger, L.J. Hardwick, J.-M. Tarascon, Nat. Mater. 11 (2011) 19–29.
[6] A. Zhamu, G.R. Chen, C.G. Liu, D. Neff, Q. Fang, Z.N. Yu, W. Xiong, Y.B. Wang, X.Q. Wang, B.Z. Jang, Energy Environ. Sci. 5 (2012) 5701–5707.
[7] W. Xu, J. Wang, F. Ding, X. Chen, E. Nasybulin, Y. Zhang, J.-G. Zhang, Energy Environ. Sci. 7 (2014) 513–537.
[8] S. Chandrashekar, N.M. Trease, H.J. Chang, L.S. Du, C.P. Grey, A. Jerschow, Nat. Mater. 11 (2012) 311–315.
[9] G. Girishkumar, B. McCloskey, A. Luntz, S. Swanson, W. Wilcke, J. Phys. Chem. Lett. 1 (2010) 2193–2203.
[10] B. Scrosati, J. Garche, J. Power Sources 195 (2010) 2419–2430.
[11] E. Zinigrad, E. Levi, H. Teller, G. Salitra, D. Aurbach, P. Dan, J. Electrochem. Soc. 151 (2004) A111–A118.
[12] J.L. Schaefer, Y. Lu, S.S. Moganty, P. Agarwal, N. Jayaprakash, L.A. Archer, Appl. Nanosci. 2 (2012) 91–109.
[13] D. Aurbach, I. Weissman, A. Zaban, O. Chusid, Electrochim. Acta 39 (1994) 51–71.
[14] A. Ritchie, J. Power Sources 96 (2001) 1–4.
[15] R. Rauh, S. Brummer, Electrochim. Acta 22 (1977) 75–83.
[16] K. Abraham, J. Elliot, J. Electrochem. Soc. 131 (1984) 2211–2217.
[17] K. Zaghib, M. Armand, M. Gauthier, J. Electrochem. Soc. 145 (1998) 3135–3140.
[18] S. Liu, N. Imanishi, T. Zhang, A. Hirano, Y. Takeda, O. Yamamoto, J. Yang, J. Electrochem. Soc. 157 (2010) A1092–A1098.
[19] B. Scrosati, A. Selvaggi, F. Croce, W. Gang, J. Power Sources 24 (1988) 287–294.
[20] R. Xue, H. Huang, X. Huang, L. Chen, Solid State Ionics 74 (1994) 133–136.
[21] Y. Gofer, M. Ben-Zion, D. Aurbach, J. Power Sources 39 (1992) 163–178.
[22] D. Aurbach, E. Zinigrad, H. Teller, Y. Cohen, G. Salitra, H. Yamin, P. Dan, E. Elster, J. Electrochem. Soc. 149 (2002) A1267–A1277.
[23] D. Aurbach, E. Zinigrad, H. Teller, P. Dan, J. Electrochem. Soc. 147 (2000) 1274–1279.
[24] F. Ding, W. Xu, G.L. Graff, J. Zhang, M.L. Sushko, X. Chen, Y. Shao, M.H. Engelhard, Z. Nie, J. Xiao, J. Am. Chem. Soc. 135 (2013) 4450–4456.
[25] J.S. Lee, S. Tai Kim, R. Cao, N.S. Choi, M. Liu, K.T. Lee, J. Cho, Adv. Energy Mater. 1 (2011) 34–50.
[26] D. Aurbach, J. Power Sources 89 (2000) 206–218.
[27] L. Yang, C. Smith, C. Patrissi, C.R. Schumacher, B.L. Lucht, J. Power Sources 185 (2008) 1359–1366.
[28] D. Aurbach, Y. Gofer, J. Langzam, J. Electrochem. Soc. 136 (1989) 3198–3205.
[29] D. Aurbach, Y. Talyosef, Boris Markovsky, Elena Markevich, E. Zinigrad, L. Asraf, J.S. Gnanaraj, H.-J. Kim, Electrochim. Acta 50 (2004) 247–254.
[30] S.A. Freunberger, Y. Chen, N.E. Drewett, L.J. Hardwick, F. Bardé, P.G. Bruce, Angew. Chem. Int. Ed. 50 (2011) 8609–8613.
[31] W. Wang, Y. Wang, Y. Huang, C. Huang, Z. Yu, H. Zhang, A. Wang, K. Yuan, J. Appl. Electrochem. 40 (2010) 321–325.
[32] P.C. Howlett, D.R. MacFarlane, A.F. Hollenkamp, Electrochem. Solid-State Lett. 7 (2004) A97–A101.
[33] L. Suo, Y.-S. Hu, H. Li, M. Armand, L. Chen, Nat. Commun. 4 (2013) 1481–1489.
[34] L. Li, S. Zhou, H. Han, H. Li, J. Nie, M. Armand, Z. Zhou, X. Huang, J. Electrochem. Soc. 158 (2011) A74–A82.
[35] H.-B. Han, S.-S. Zhou, D.-J. Zhang, S.-W. Feng, L.-F. Li, K. Liu, W.-F. Feng, J. Nie, H. Li, X.-J. Huang, J. Power Sources 196 (2011) 3623–3632.
[36] A.S. Best, A.I. Bhatt, A.F. Hollenkamp, J. Electrochem. Soc. 157 (2010) A903–A911.
[37] W. Wei, J. Wang, L. Zhou, J. Yang, B. Schumann, Y. NuLi, Electrochem. Commun. 13 (2011) 399–402.
[38] P. Howlett, N. Brack, A. Hollenkamp, M. Forsyth, D. MacFarlane, J. Electrochem. Soc. 153 (2006) A595–A606.
[39] A. Budi, A. Basile, G. Opletal, A.F. Hollenkamp, A.S. Best, R.J. Rees, A.I. Bhatt, A.P. O'Mullane, S.P. Russo, J. Phys. Chem. C 116 (2012) 19789–19797.
[40] S. Shiraishi, K. Kanamura, Z.-i. Takehara, Langmuir 13 (1997) 3542–3549.
[41] S. Shiraishi, K. Kanamura, Z.i. Takehara, J. Electrochem. Soc. 146 (1999) 1633–1639.
[42] E. Peled, D. Golodnitsky, G. Ardel, J. Electrochem. Soc. 144 (1997) L208–L210.